Joint Occurrence of Heavy PM$_{2.5}$ Pollution Episodes and Persistent Foggy Days in Central East China

Caixia Yu [1,2,3,4], Yuanjian Yang [5] and Dong Liu [2]*

[1]Key Laboratory of Atmospheric Optics, Anhui Institute of Optics and Fine Mechanics Chinese Academy of Sciences, Hefei Institutes of Physical Science, Chinese Academy of Sciences, Hefei, China, [2]Science Island Branch, Graduate School of USTC, Hefei, China, [3]Anhui Province Key Laboratory of Atmospheric Sciences and Satellite Remote Sensing, Anhui Institute of Meteorological Sciences, Hefei, China, [4]Shouxian National Climate Observatory, Typical Farmland Eco-Meteorology Field Scientific Test Base of China Meteorological Administration in Huaihe River Basin, Shouxian, China, [5]School of Remote Sensing and Geomatics Engineering, Nanjing University of Information Science and Technology, Nanjing, China

Although many severe pollution events in Central and East China have been analyzed in recent years, the heavy PM$_{2.5}$ pollution episode happened on persistent foggy days from January 13 to 18, 2018 was unique, characterized by explosive increase and sharp decrease in PM$_{2.5}$ (particles with kinetic equivalent diameter less than or equal to 2.5 microns) concentration. Based on hourly data of ground level meteorological parameters, PM$_{2.5}$ data and CALIPSO-based (the Cloud-Aerosol Lidar and Infrared Pathfinder Satellite Observation) aerosol data, combined with ECMWF (European Centre for Medium-Range Weather Forecasts) reanalysis data and radiosonde temperature profile, a comprehensive analysis was conducted to reveal the meteorological reasons for the evolution of the episode at horizontal and vertical scales. The PM$_{2.5}$ concentration experienced four stages: a slow-increase phase, rapid-increase phase, rapid-decrease phase, and rebound phase. Results show that because Central and East China (CEC) were located at the back of a high-pressure system, humid southerly winds and near surface inversion (NSI) were responsible for the slow accumulation of pollutants. The rapid-increase phase was attributed to pollution transport at both ground level and in the lower troposphere because of weak cold air invasion. The significant subsidence at 500 hPa and 700 hPa intensified the NSI and led to dense fog. In that case, corresponding to the supersaturated atmosphere, the particles entered the fog droplets and were scavenged partly by deposition at night and were resuspended on the next day when the atmosphere was unsaturated. Our findings provide convincing evidence that surface PM$_{2.5}$ rapid-decrease phase and the rebound phase were closely associated with dense fog process.

Keywords: PM$_{2.5}$ pollution episodes, fog process, wet deposition, subsidence motions, rebound

INTRODUCTION

In recent years, severe air pollution events have received media and public coverage as common phenomena in China (Guo et al., 2011; Ding and Liu, 2014; Wang et al., 2019). High particulate matter levels are usually closely associated with high levels of precursor emissions (Markovici et al., 2014; Holt et al., 2015). Therefore, the government took strong measures to improve those enterprises with high energy consumption, such as coal, to reduce pollution emissions (Liu

et al., 2015; Guo et al., 2016; Gao et al., 2020). However, according to the statistics, humans still suffer from air pollution during most of the wintertime in some Chinese cities (Chen et al., 2013; Yang et al., 2020). Especially in the Beijing-Tianjin-Hebei region (BTH) and Yangtze River Delta region (YRD), large amounts of data indicate that air pollution has been very serious as a consequence of the phenomenal economic growth (Zhang et al., 2012; Wang et al., 2015; Zhang et al., 2015; Zheng et al., 2018). Fine particles suspended in the air contain high concentration of heavy metals, which enter the blood circulation through the respiratory system and then result in disease (Peters et al., 1996; Delfino et al., 2005; Pope and Dockery, 2006; Wei et al., 2017; Gu et al., 2020), which vitally affects social activities.

The formation mechanisms of typical $PM_{2.5}$ pollution episodes over China have been extensively studied to provide references for local governments to take air pollution control measures (Gao et al., 2012; Zhou et al., 2015; Jin et al., 2017; Wu et al., 2020; Wang, et al., 2021a; Wang, et al., 2021b). Normally, meteorological factors play a significant role in the generation, development and end of pollution events through a complex combination of processes, including pollutant transitions, secondary particle production, particle hygroscopic growth and wet removal processes, and are principally responsible for heavy pollution episodes (Pasch et al., 2011; Wang and ChenSun, 2014; Wang et al., 2015; Miao et al., 2017; Yang et al., 2018). Many studies have been carried out to understand the correlation between climate and pollution episodes in China (Zhu et al., 2012; Li et al., 2016; Yang et al., 2018). It is generally believed that the weakening East Asia winter monsoons result in reductions in the number of strong cold outburst events and increases in stagnant weather conditions, both of which further lead to more heavy pollution events (Lin et al., 2018). In addition, studies have shown that pollutant accumulations are directly influenced by local adverse meteorological parameters (Chen et al., 2008; Deng et al., 2012; Ji et al., 2014). It has been indicated that reduced rainfall amounts, gentle winds and high relative humidity are key factors in the formation of heavy pollution (Sun et al., 2013; Shi et al., 2018; Chen et al., 2020).

Meanwhile, wet deposition of particulate matter caused by precipitation and fog are also important process to purified air and maintain the source-sink balance of suspended particles in the atmosphere. Previous studies reported that the air quality deteriorated during haze but improved in fog (Wang and ChenSun, 2014; Xu et al., 2017). Especially in the late stage of extremely dense fog episodes, particulate mass concentration reached the lowest value because of the progressive accumulated effect of wet deposition of large fog droplets (Yang et al., 2012). The observations showed also that in a core city of BTH region, the concentrations of $PM_{2.5}$ and SO2 obviously decreased during the heavy fog period (Han et al., 2018). Compared with dry deposition, the wet deposition by fog formation led to pollutant lifetimes on the order of 6–12 h, while pollutant removal by ventilation of valley air required at least 5 days (Waldman and Hoffmann, 1987).

CEC lies in the north and south climate intermediate belts with time-varying weather conditions, and both increase the difficulty of studying pollution episodes. The formation and

FIGURE 1 | The topography of Central East China, locations of representative cities and the CALIPSO satellite orbit used in this paper. The red letters indicate provinces (e.g., SX: Shanxi, HeB: Hebei, SD: Shandong, HN: Henan, HuB: Hubei, AH: Anhui, and JS: Jiangsu). The pink spot indicates a city (fy: Fuyang). The blue spots indicate the CALIPSO satellite orbit that passed over CEC on January 16.

evolution of heavy $PM_{2.5}$ pollution episodes are characterized by distinctive regional features. Even though studies have analyzed the characteristics and mechanisms of heavy $PM_{2.5}$ pollution episode in CEC, few studies have reported the joint occurrence of persistent $PM_{2.5}$ pollution episodes and foggy days. In this paper, the heavy air pollution episode accompanied by dense fog in CEC was taken as an example to comprehensively analyze the driving meteorological conditions for slow-increase, rapid-increase and short-term dissipation of $PM_{2.5}$ pollution by using meteorological data (including high-resolution sounding data, surface observation data, and reanalysis data); real-time pollutant concentration monitoring data; and vertical aerosol extinction coefficient data that were monitored by CALIPSO.

DATA AND METHODS

Region and Site

Severe $PM_{2.5}$ pollution episodes occurred in central and eastern China (mainly in Shanxi, Hebei, Shandong, Henan and Anhui provinces) during January 13–18, 2018. In addition, Fuyang was selected as the representative city in this paper. Fuyang (115.82°E, 32.92°N, 39 m above sea level) is located in northwestern Anhui Province and has a seasonal temperate semi humid monsoon climate (Deng et al., 2019). The monsoon climate is clearly defined with concentrated rainy summers and cold winters. Northerly winds rule in winter, while southerly winds prevail in summer. Fuyang station possesses a modern observation system that can conduct surface meteorological observations and sounding measurements and provides abundant and reliable observational data for relevant research.

Air Quality Data

All the data and results in this study were presented at Beijing Standard Time (BST). The PM$_{2.5}$ hourly concentration data were downloaded from the website of the Ministry of Environmental Protection of China. Based on the PM$_{2.5}$ concentration, heavy air pollution was found to occur in central and eastern China on January 13–18 and accompanied by large-scale dense fog. During this episode, the areas with PM$_{2.5}$ concentration greater than 150 μg/m^3 expanded and moved southward. In addition, the characteristics of the pollutant concentration at different stages and their relationships with the meteorological parameters were analyzed, which included slow increases, rapid increases and sharp decreases in PM$_{2.5}$ concentration. **Figure 1** shows the topography of CEC and the surrounding areas and the location of the representative city, Fuyang, which experienced violent swings in the PM$_{2.5}$ concentration during January 13–18.

Meteorological Data

The circulation patterns and vertical motions of the middle-lower troposphere are closely related to the surface meteorological conditions. The sea level pressure (SLP) and vertical velocity data with a resolution of 0.25°* 0.25° obtained from the ECMWF were obtained from the European Centre for Medium-Range Weather Forecasts were used to analyze the influence of the weather systems during the severe pollution episode.

To understand the effects of surface meteorological parameters on pollutant concentration, hourly ground meteorological observation data and sounding data from Fuyang station were obtained from the Anhui Information Center of Meteorology, where data quality control had been carried out and were utilized in the study. The surface meteorological variables included hourly ground level temperature, dew point temperature, wind speed, wind direction, relative humidity and visibility. The high-resolution (1.2 s) sounding data that were obtained at 07:00 and 19:00 at the Fuyang sounding station were used to determine the temperature inversions and vertical wind distributions. The accuracies of the radiosonde temperature data are within 0.1 K and have been broadly used to characterize the boundary layer structures in China (Guo et al., 2019). These observations are conducted by specially trained personnel and use the procedures established by the World Meteorological Organization (WMO).

CALIPSO Data

During the study period, CALIPSO passed over the contaminated area. The CALIOP instrument was launched in 2006 and has provided nearly continuous global measurements of aerosols and clouds with high vertical and spatial resolutions (David et al., 2009), which are important for studies of radiative forcing (Satheesh, 2002) and air quality (Al-Saadi et al., 2005). The level 2 products are reported both as layer products and as profile products. In this paper, the version 3.01 level 2 aerosol layer product was used to obtain the altitude-height distributions of the aerosol extinction coefficients and further investigate the vertical distributions of the aerosols. The product has a horizontal resolution of 333 m and vertical resolution of 30 m below 8 km.

THE POLLUTION PROCESS AND DENSE FOG EVENT

Spatiotemporal Variations in PM$_{2.5}$ Concentration

Figure 2 depicts the PM$_{2.5}$ concentration distributions at 06:00 for each day during January 13–18, 2018. We observed that a heavy pollution zone PM$_{2.5}$ > 150 μg/m^3) began in Shanxi Province on January 13 and worsened the next day. On January 15, the heavily contaminated area moved eastward to the BTH region and expanded southward to the border with Shandong and Hebei Provinces. On the morning of January 16, we found that the pollution zone moved southward and that the center of heavy pollution was located at the region where Henan, Shandong and Hubei Provinces intersect. On January 17, the heavily polluted area moved further southward and the air quality in eastern Hebei Province was improved, while the PM$_{2.5}$ concentration for most parts of Henan rose to above 250 μg/m^3. Meanwhile, it should be noted that PM$_{2.5}$ concentration in northwest Anhui, where the Fuyang sounding station is located, sharply decreased to below 100 μg/m^3 at 06:00 January 17. The air quality exhibited large differences between southeastern Henan and northwestern Anhui.

Previous studies have shown that cold air intrusion and precipitation are the main removal mechanisms of large-scale severe pollution (Kang et al., 2019), especially in winter. However, improvements in air quality occurred in limited areas with no precipitation at 06:00 January 17, while the pollution in the surrounding areas remained, which indicated that local meteorological parameters played a role during the episode. On January 18, the pollutants again remained in the atmosphere above Henan, Shandong and their border with Anhui and Jiangsu Provinces.

The whole pollution process led to average PM$_{2.5}$ concentration reach 120 μg/m^3 from 04:00 January 13 to 04:00 January 18 in Fuyang city. Time series plots of the PM$_{2.5}$ concentration are shown in **Figure 3**. We found that the PM$_{2.5}$ mass concentration evolution trend in Fuyang could be divided into four phases (**Table 1**): 1) a slow-increase phase from 04:00 January 13 to 08:00 January 16, 2) rapid-increase phase from 08:00 January 16 to 20:00 January 16, 3) rapid-decrease phase from 20:00 January 16 to 07:00 January 17, and 4) rebound phase from 07:00 January 17 to 04:00 January 18. In the first stage, the PM$_{2.5}$ mass concentration increased slowly to 139 μg/m^3 from 43 μg/m^3. The most severe PM$_{2.5}$ pollution levels occurred in the second stage, with a peak value of 285 μg/m^3 at 20:00 January 16. Thereafter, the PM$_{2.5}$ mass concentration decreased sharply to 31 μg/m^3 within 11 h. However, after short-term dissipation, the PM$_{2.5}$ mass concentration rebounded to 166 μg/m^3 in 1 day. This means that although the air quality improved quickly during the evening of January 16, the pollutants were not cleaned up.

The PM$_{2.5}$/PM$_{10}$ ratios of the mass concentration exhibited obvious differences at different stages. The ratios were always between 0.63 and 0.86 with no obvious trends during the slow-increase stage, and the ratios increased overall to 0.79–0.95 in the rapid-increase stage, which suggested that fine particles accounted for a large proportion of the particle mass.
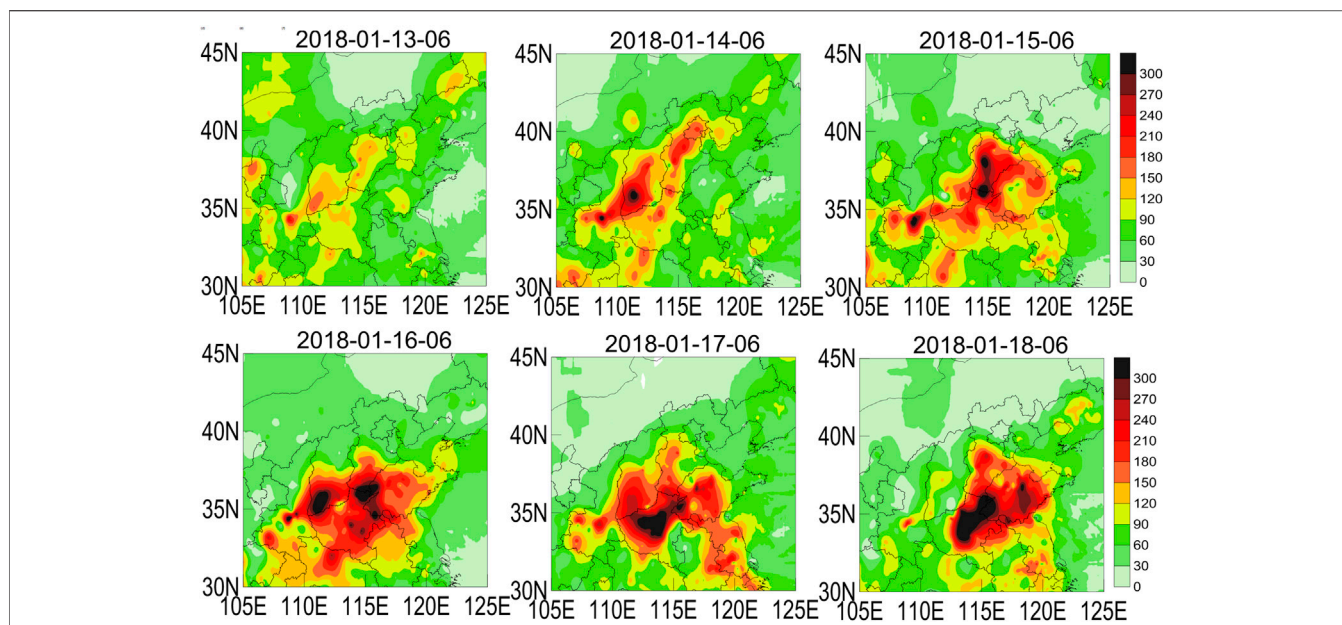
FIGURE 2 | Distributions of $PM_{2.5}$ (unit: µg/m^3) concentration at 06:00 in Central-East China on 13–18 **(A–F)** January 2018.
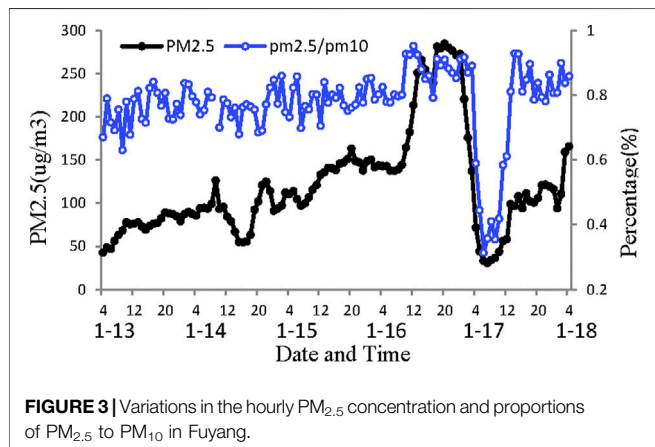

FIGURE 3 | Variations in the hourly $PM_{2.5}$ concentration and proportions of $PM_{2.5}$ to PM_{10} in Fuyang.

Thereafter, the particles exhibited irregular fluctuations, the $PM_{2.5}/PM_{10}$ ratios dropped to 0.31, and PM_{10} became the main pollutant in the rapid-decrease stage. Corresponding to the rebound in pollutant concentration in the daytime on January 17, the ratios rose to 0.93 and remained above 0.78 on January 18.

Fog Weather Process During the Episode

Fog is a weather phenomenon, which occurs when the atmospheric relative humidity in the boundary layer is greater than 90% and the horizontal visibility is less than 1 km. The visibility within 1–10 km is called light fog. It is worth noting that large-scale foggy weather was observed on the mornings of January 16–18 and affected more than 20 provinces in China. **Figure 4** depicts the dense fog areas with visibility below 1 km and the relative humidity exceeds 90%. On the morning of January 17, dense fog occurred in most parts of Anhui and Jiangsu Provinces and their border with Hebei and Shandong Provinces. Especially in northern Anhui Province, the visibility was less than 0.4 km.

THE DRIVING METEOROLOGICAL CONDITIONS FOR SLOW-INCREASE, RAPID-INCREASE AND SHORT-TERM DISSIPATION OF $PM_{2.5}$ POLLUTION

Large Scale Synoptic Patterns

Figure 5 shows that evolution of the sea level pressure fields during the heavy pollution episode. The results show that CEC

TABLE 1 | Summary of the different air pollution stages in Fuyang during the study period.

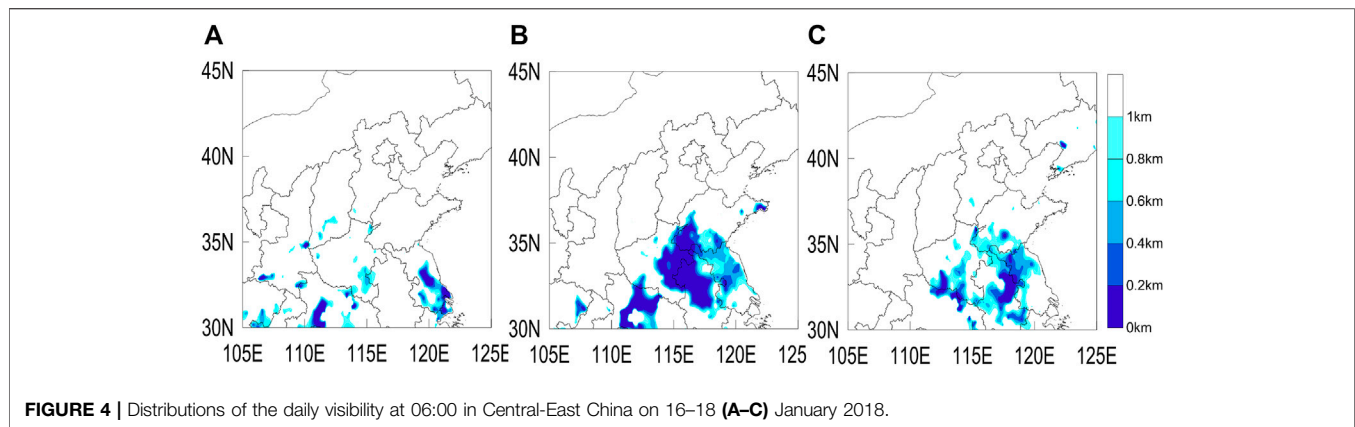| Stage	Date	Duration (h)	Initial $PM_{2.5}$ concentration (µg/m^3)	End $PM_{2.5}$ concentration (µg/m^3)	$PM_{2.5}$ difference (µg/m^3)
Slow increase	04:00 January13-08:00 January16	76	43	139	96
Rapid increase	08:00 January16-20:00 January16	12	139	285	146
Rapid decrease	20:00 January16-07:00 January17	11	285	31	-254
Rebound	07:00 January17-04:00 January18	21	31	166	135

FIGURE 4 | Distributions of the daily visibility at 06:00 in Central-East China on 16–18 (A–C) January 2018.

experienced sustained south winds due to its location near the rear of the high-pressure system that was caused by the East Asian trough on January 13 (**Figure 5A**). In addition to the East Asian trough moving east on January 14, the atmospheric circulation adjusted, as is demonstrated by the continuous high-pressure systems, and was separated from the Mongolia-Siberian High Pressure (**Figure 5B**). A separate high-pressure system centered at the Bohai Gulf area moved rapidly east on January 15 (**Figure 5C**). After that, a slightly stronger high-pressure system was separated again on the morning of January 16 and affected a wider area, while weak north winds prevailed in Anhui (**Figure 5D**). However, the high pressure system was not strong enough and gradually diminished by the night of January 16. Meanwhile, the southerly airstream strengthened and moved northward, which meant that convergence lines formed at night on January 16 in CEC when the enhanced southerly winds met the original northerly winds. By the morning of January 17, CEC was entirely dominated by southerly winds.

The changes in SLP in Anhui, along with the surface winds, demonstrate that heavy pollution episodes occurred during the atmospheric circulation adjustment period, with several weak colds fronts intruding into the North China Plain and Northeast Plain. Most of the time, the SLP were uniformly distributed, with southerly wind speeds that were low in CEC.
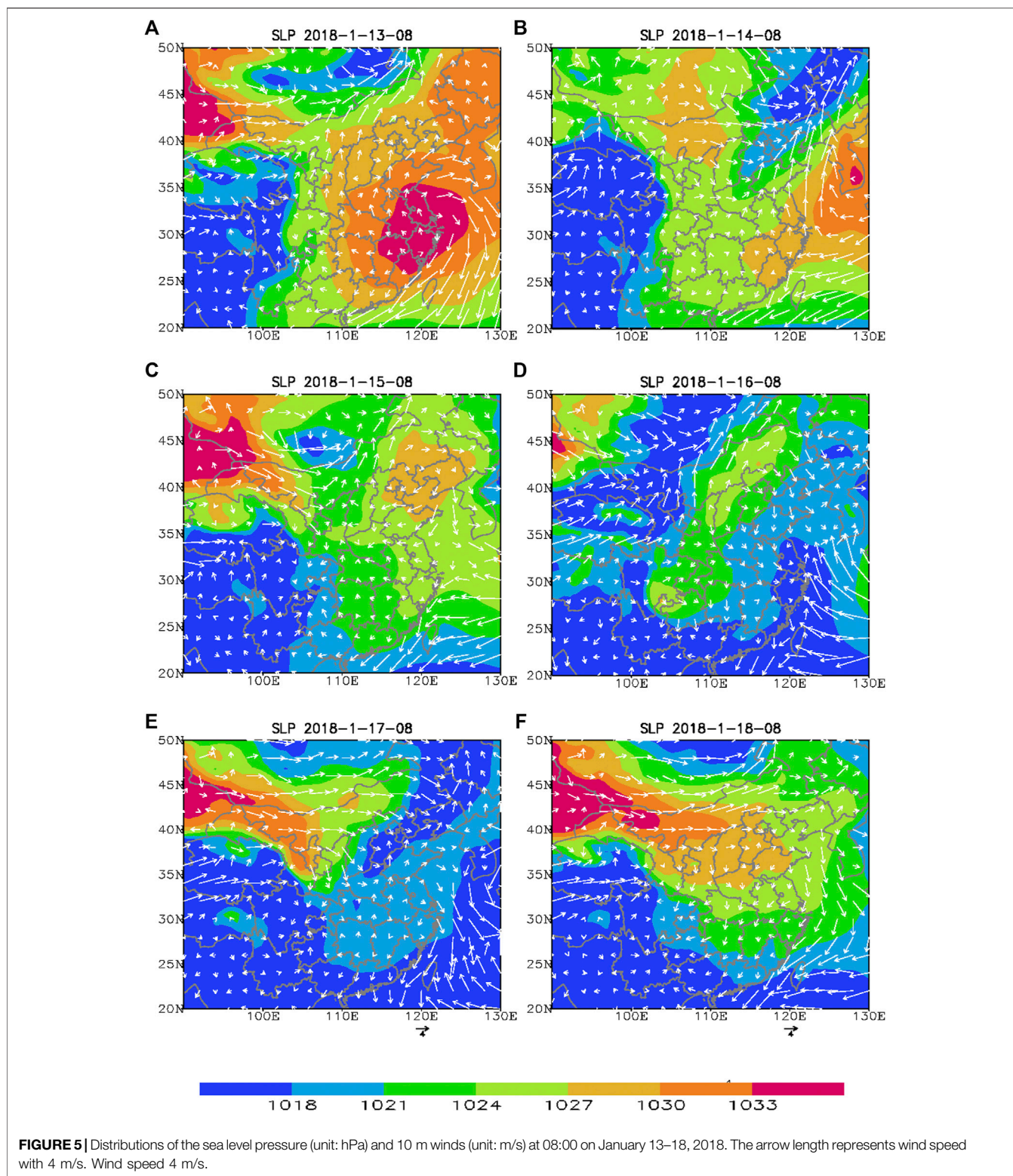
Inversion of Boundary Layer Temperature

The wind and temperature profiles at the Fuyang sounding station that were obtained at 07:00 and 19:00 on each day during the episode were used to reveal the vertical structures of the atmospheric layer (**Figure 6**). On January 13–14, all of the middle and lower troposphere was controlled by southwesterly winds. In particular, the southwesterly warm moisture flow was stronger between 500 m and 1,500 m (**Figure 6A**), which led to the temperature of the lower atmosphere being higher than that at the surface. Therefore, an NSI was observed in the morning and night of January 13–14 (**Figures 6B,C**). The top of the NSI was below 500 m, and its intensity was approximately 1–2.4°C/100 m. These results indicate that a persistent temperature inversion decreased the thickness of the mixing layer and hindered the upward transport of pollutants and was favorable for the gradual air pollution accumulation on the ground at the early stage of the pollution episode.

The prevailing wind direction within 1 km of the ground shifted to northeast on the evening of January 15 (**Figure 6A**). At 07:00 on January 16, northerly winds further strengthened and dominated from ground level to 3 km or higher, which indicated that the warm air mass had weakened and retreated southward when the cold air mass was enhanced and the CEC area was controlled. The northerly wind broke the NSI and an inversion layer appeared between 1,400 and 1,500 m, which was higher in the daytime on January 16 (**Figure 6E**).

Although the vertical diffusion conditions improved, the ground pollution levels were pushed upward (**Figure 3**). Therefore, we further investigated the effect of pollutant transport in the daytime of January 16. **Figure 7** shows the height-latitude cross section of aerosol extinction along the orbit displayed in **Figure 1** on 13:00 January 16. After removing the influence of clouds, the high extinction coefficients were attributed to high aerosol concentration. Large amounts of aerosols were distributed from the ground up to 1.5 km between 31.5°N and 35°N. As mentioned in **Figures 5D**, **6A**, not only the surface but also the lower atmosphere were controlled by north winds in Anhui and Henan Provinces as a result of the development of the high-pressure system. It can be deduced that in addition to pollution transport on the ground, the north winds in the lower atmosphere were also conducive to the transport of particulate matter from North China to CEC during the episode.

On the morning of January 17 (07:00), corresponding to the northerly winds at ground level up to 1.5 km and southwesterly winds above 2 km, the ground temperature dropped to 0°C, but the temperature at 1,500 m rose from −3°C to 3°C and formed a deep, strong SBI in the boundary layer with the inversion top located at approximately 200 m and the top of the isothermal layer at approximately 2 km. The SBI at 07:00 January 17 decreased the thickness of the mixing layer and was favorable for the accumulation of air pollution on the ground. However, under unfavorable conditions, the PM$_{2.5}$ mass concentration at Fuyang decreased sharply and decreased by 254 µg/m³ within 11 h (**Table 1**). We further investigate the reasons for the sharp reduction in PM$_{2.5}$ concentration in *Analysis of the Reasons for the Dramatic Drop and Rebound in PM$_{2.5}$ Concentration*. At the night of January 17 (**Figure 6F**), the surface temperature rose from 0°C to about 4°C, but the NSI was not broke. The top of the isothermal layer located at approximately 2 km.

FIGURE 5 | Distributions of the sea level pressure (unit: hPa) and 10 m winds (unit: m/s) at 08:00 on January 13–18, 2018. The arrow length represents wind speed with 4 m/s. Wind speed 4 m/s.

Surface Meteorological Factors

To further understand the formation, maintenance and short-term dissipation of the episode, especially the two increasing phases and one sharp reduction phase, extensive analyses were conducted to understand the driving meteorological conditions. Hence, the hourly near-surface meteorological conditions (e.g., wind speed, wind direction, temperature, dew point temperature, relative humidity, and visibility) and important weather events
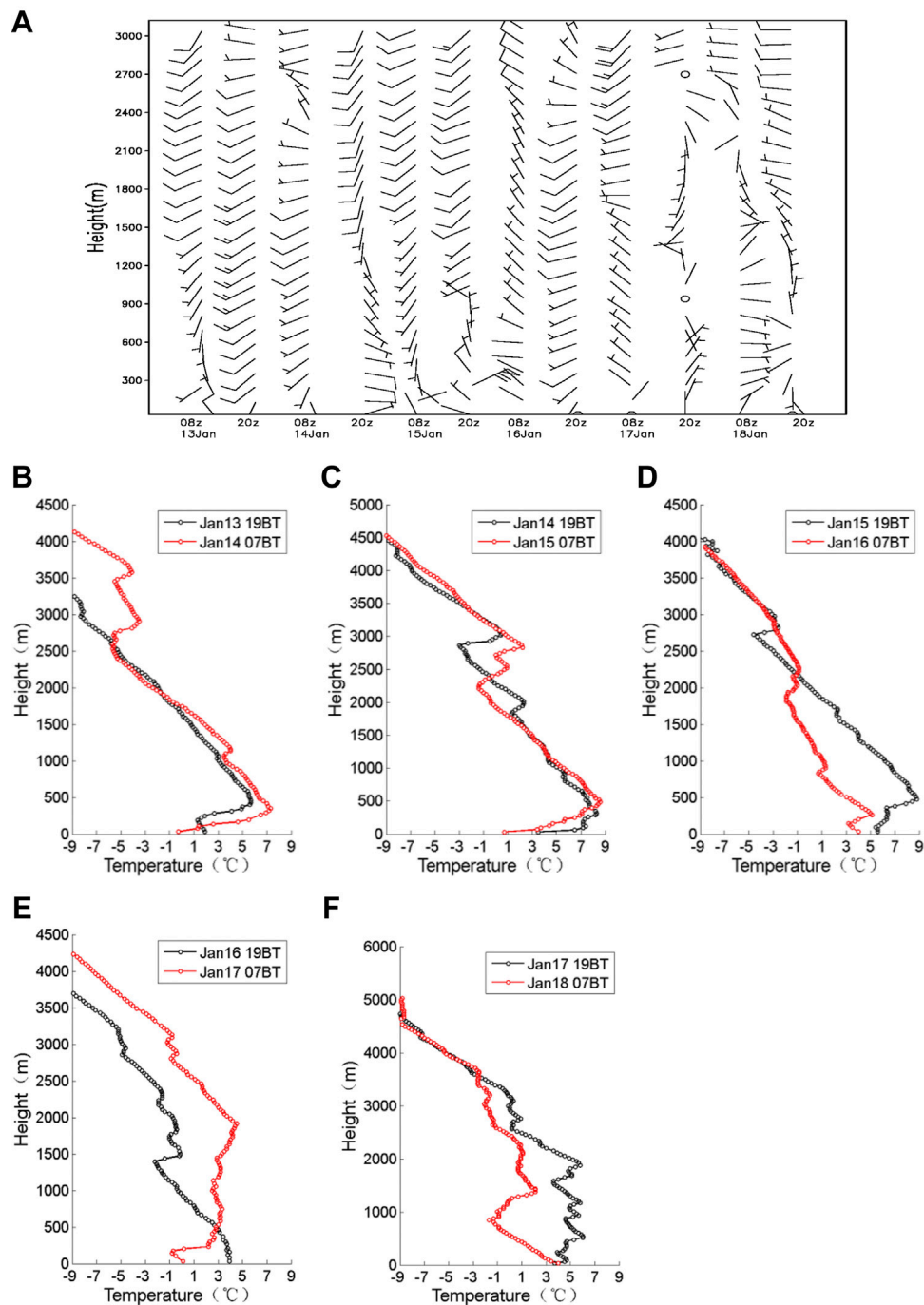
FIGURE 6 | Vertical distributions of wind vector **(A)** and temperature **(B–F)** at the Fuyang sounding station, which are shown in **Figure 1**, from January 13 to January 18, 2018.

from January 13 to January 18, 2018 in Fuyang are shown in **Figure 8**.

In the early period of the slow-increase stage (January 13–14), the prevailing wind direction was mainly southeast on January 13–14 with wind speeds of approximately 2–3 m/s. The ground relative humidity correspondingly showed fluctuating growth and reached

90% at 00:00 on January 15 (**Figure 8B**). In combination with **Figures 6**, **8A**, it can be deduced that the existence of the NSI led to pollutants being confined to the shallow mixing layer, and the sustained southerly winds increased the moisture content of the atmosphere and particle hygroscopic growth occurred, which were both conducive to an increase in the $PM_{2.5}$ mass concentration. In the
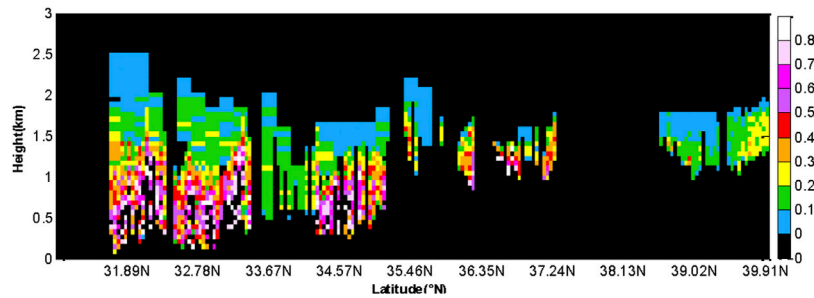
FIGURE 7 | Vertical distribution of the aerosol extinction coefficients along the CALIPSO orbit at 13:00 January 16.

later period of the slow-increase stage (January 15), the prevailing wind speeds were light, and the directions changed frequently from southeast to northeast due to a weak high-pressure system that originated in Mongolia (**Figure 8C**). This meant that the enhanced northerly winds met the southerly winds and the wind fields converged near Fuyang, which led to the pollutants and vapor that had been transported in the earlier stage remaining for a longer period and were not conducive to the diffusion of pollutants.

On January 16, due to the development of the high-pressure system shown in **Figure 5D**, weak cold air invaded southward, and

north winds prevailed on the ground with velocities below 2 m/s in Fuyang (**Figure 8A**). It is worth noting that the center of highest pollution was located in the region north of Fuyang, so it transported pollutants from Henan and Shandong. However, the cold air was so weak that the pollutants in CEC could not be carried away and continued to accumulate. Meanwhile, along with a sharp increase in the $PM_{2.5}$ mass concentration, the visibility further decreased to less than 1 km by 17:00 January 16.

It could not be neglected that the value of relative humidity increased gradually from January 13 to 15 (**Figure 8B**). At the night
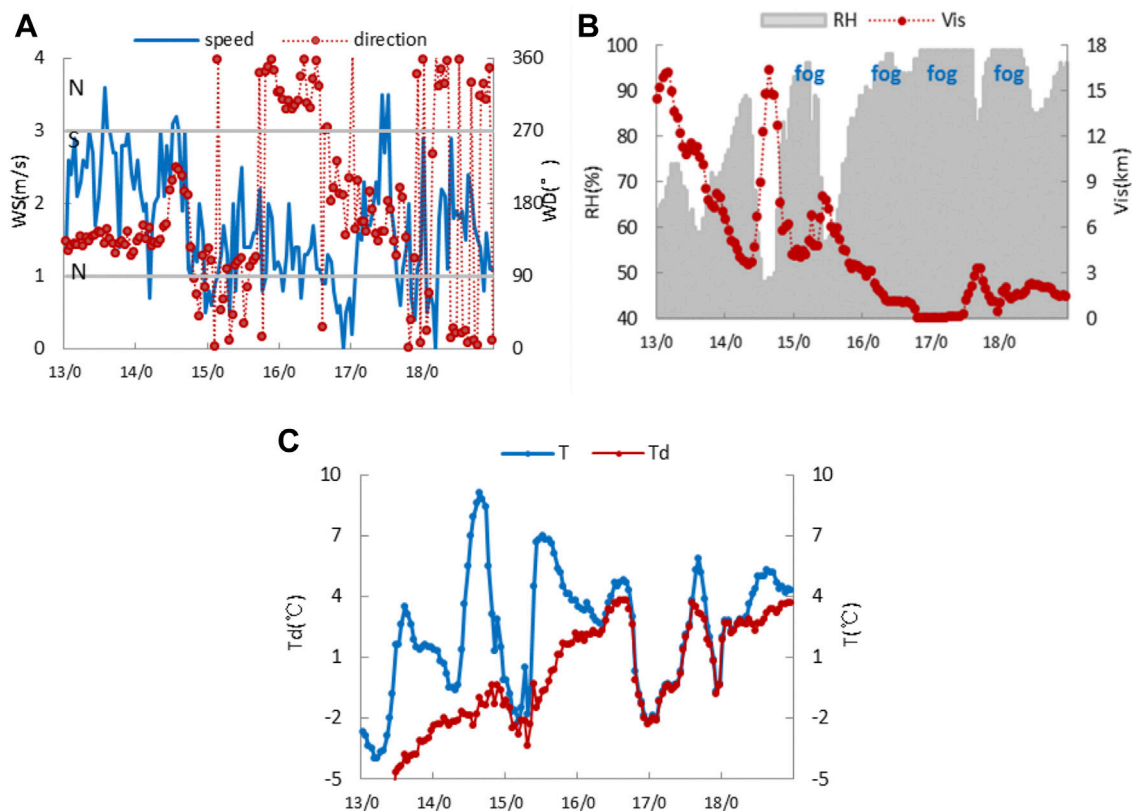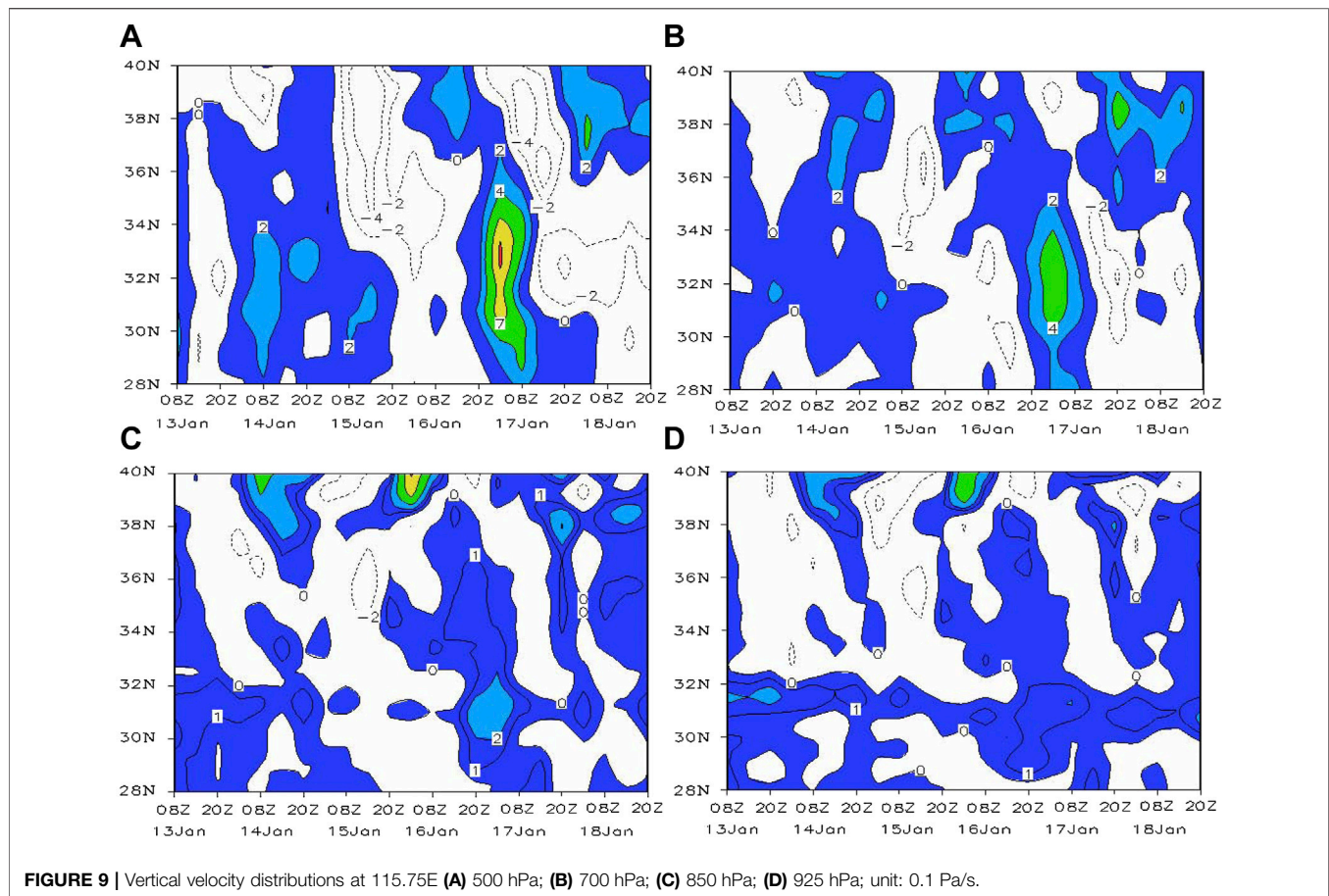

FIGURE 8 | Hourly surface meteorological conditions from January 13 to January 23, 2018 at Fuyang station including **(A)** wind speeds (WS), wind directions (WD), **(B)** relative humidity (RH) and visibility (Vis), **(C)** temperature (T) and dew point temperature (Td).

FIGURE 9 | Vertical velocity distributions at 115.75°E **(A)** 500 hPa; **(B)** 700 hPa; **(C)** 850 hPa; **(D)** 925 hPa; unit: 0.1 Pa/s.

of January 14, the relative humidity exceeded 90% and haze turned into light fog. However the fog days just sustained for about 7 h and then dissipated as the sun rose. At the afternoon of January 16, because of the weakening of the high-pressure system, the surface winds changed to the south in Fuyang which brought warm, moist air, which resulted in relative humidity greater than 95% by the evening of January 16 and maintained at a high level over the next few days. From 08:00 January 16 to 14:00 January 17, the dew point temperature was nearly equal to the temperature, and the air was totally saturated (**Figure 8C**). Therefore, psersistant fog days were observed in Fuyang and surrounding areas during January 16–18, as shown in **Figure 4B**. Especially at the night of January 16, the visibility was below 300 m, which meant dense fog formed. It should be noted that it was during that time that the $PM_{2.5}$ mass concentration dropped to 31 μg/m³ from 285 μg/m³. Therefore, it can be deduced that the dense fog played an important role in the sharp decline in $PM_{2.5}$ concentration during the pollution episode.
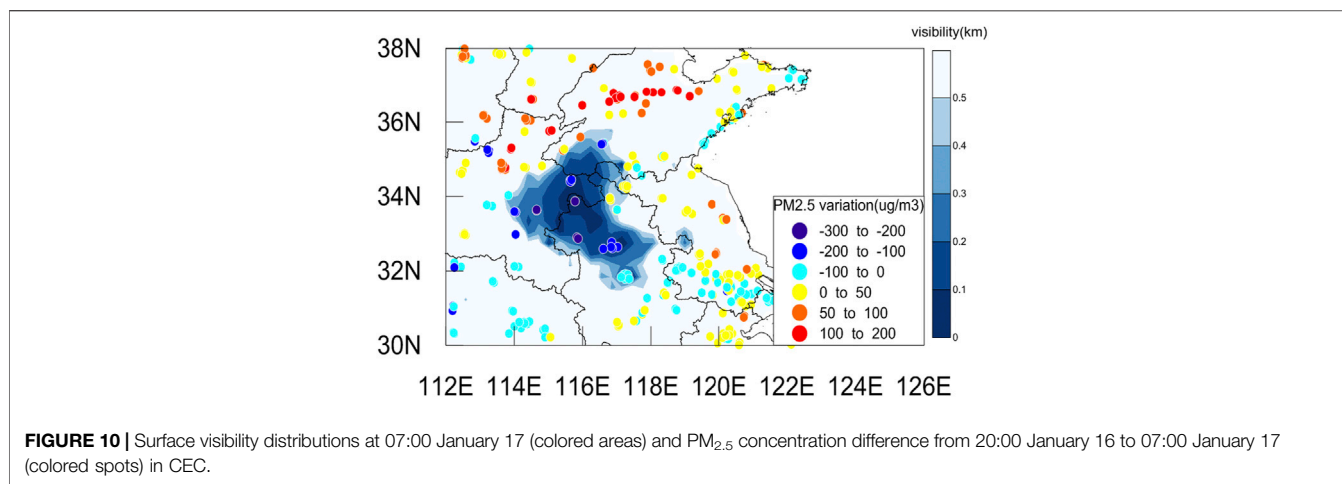
Analysis of the Reasons for the Dramatic Drop and Rebound in $PM_{2.5}$ Concentration

As mentioned above (**Figures 6**, **7**), the meteorological characteristics in Fuyang from 20:00 January 16 to 07:00 January 17 can be summarized as a strong NSI, high humidity, and ground breeze, none of which were conducive to pollution dissipation (He

et al., 2017). Therefore, we further investigated the reason for the sudden pollution decrease on the night of January 16.

Figure 9, shows the time-latitude cross sections of the vertical velocities at 500, 700, 850, and 925 hPa along 115.75°E (Fuyang Station 115.82°E, 32.92°N). The results show that significant subsidence occurred from the evening of January 16 to the morning of January 17 in the mid-low troposphere and that the center was located at 33°N. The greatest subsidence speed at 500 hPa was approximately 1.0 Pa/s, which decreased to 0.4 Pa/s at 700 hPa and was weaker and not obvious at 850 and 925 hPa. The local subsidence motions at 500 and 700 hPa led to a temperature increase in the lower atmosphere, and a strong NSI occurred. This is consistent with previous research results. Gramsch et al. (2014), Shi et al. (2019) suggested that subsidence movements in the middle and upper layers cause warming in the lower troposphere, and an inversion layer then forms. As a result, the strong NSI confined the vapor water to the shallow mixing layer, and large-scale fog occurred.

In **Figure 10**, the colored areas show the dense fog regions with surface visibility below 500 m at 06:00 January 17. The heavier the fog, the lower the visibility. The region of dense fog was located in the region of the intersection of Shandong, Hebei and Anhui. In Fuyang, the visibility was lower than 100 m. The colored spots depict the $PM_{2.5}$ concentration differences between 20:00 January 16 and 07:00 January 17. Negative

FIGURE 10 | Surface visibility distributions at 07:00 January 17 (colored areas) and PM$_{2.5}$ concentration difference from 20:00 January 16 to 07:00 January 17 (colored spots) in CEC.

values indicate decreases in the PM$_{2.5}$ concentration. The PM$_{2.5}$ concentration in the region of the intersection of Shandong, Hebei and Anhui experienced the largest drop with a concentration decrease that exceeded 100 μg/m^3 within 11 h. Especially in Fuyang city, Bozhou city of Anhui Province and Zhoukou city of Henan Province, the PM$_{2.5}$ concentration fell by more than 200 μg/m^3, which meant that sharp reductions occurred in the areas where dense fog appeared. It can be deduced that the scavenging of particles was caused by fog droplet deposition.

Previous research has shown that large fractions of the pollutants scavenged in fog could be removed from the atmosphere so that the occurrence of fog could diminish or limit the accumulation of particulate matter in stagnant air masses (Jacob et al., 1984). Studies have revealed that many air pollutants are deposited *via* fog droplets, and the nitrogen deposition rate *via* fog water is of the same magnitude as that *via* rainwater (Igawa et al., 1998). Moreover, a simple formula for cleaning a polluted atmosphere by fog (haze) events was deduced for fog that lasts more than 4 h (Podzimek, 1998). As mentioned above (**Figure 8**), the atmosphere was supersaturated and condensed from fog droplets on the evening of January 16. The particles entered the fog droplets and were scavenged partly by the deposition of large droplets on the surface.

On the morning of January 17, the air quality was good with PM$_{2.5}$ concentration sustained in the range of 31–58 μg/m3. At 14:00 of January 17, the relative humidity decreased to about 80% and the atmosphere was unsaturated (**Figure 8B**), the droplets dehydrated, and the aerosol particles resuspended again in the atmosphere. It resulted in a rebound in the mass concentration with the PM$_{2.5}$ concentration jumped to about 100 μg/m^3 at 14:00 of January 17 (**Figure 3**). Thereafter the air quality continued to deteriorate and started another pollution process under the unfavorable meteorological conditions.

CONCLUSION

Based on multisource observations, the characteristics and mechanisms of the heavy PM$_{2.5}$ pollution episode that was

accompanied by dense fog that occurred in CEC from January 13 to 18, 2018 were comprehensively investigated. The results showed that the episode occurred during an atmospheric circulation adjustment and that the surface PM$_{2.5}$ concentration slowly increased in Fuyang city in four stages: 1) the slow-increasing phase, 2) the rapid-increasing phase, 3) the rapid-decreasing phase, and 4) the rebound phase. The slow-increase phase was due to high humidity, ground breeze and a surface-based inversion, whereas the rapid-increase phase was due to pollution transport. In particular, the CALIPSO satellite monitoring suggested that pollution transport occurred not only at ground level but also in the lower troposphere.

The rapid-decrease phase and rebound phase were closely associated with the dense fog process. A rapid decrease in PM$_{2.5}$ concentration occurred in the region of the intersection of Shandong, Hebei and Anhui, where dense fog was observed. The analysis showed that the significant subsidence at 500 and 700 hPa led to a strong NSI, which confined the vapor water to the shallow mixing layer, and the atmosphere was supersaturated. Under these conditions, the particles entered the fog droplets and were scavenged partly by deposition of the large droplets on the surface. However, the aerosol particles were resuspended when the atmosphere was unsaturated Kang et al., 2019, Ni et al., 2018, Su et al., 2020, Wang et al., 2017, Wang et al., 2021c, Wang et al., 2014, Wang et al., 2016, Xu and Zhu, 2017, Xu et al., 2015, Zheng et al., 2019.

DATA AVAILABILITY STATEMENT

The original contributions presented in the study are included in the article/Supplementary Material, further inquiries can be directed to the corresponding author.

AUTHOR CONTRIBUTIONS

CY wrote the first draft of the manuscript, YY contributed to manuscript revision, DL contributed to conception and design of

the study. All authors contributed to manuscript revision approved the submitted version.

REFERENCES

Al-Saadi, J., Szykman, J., Pierce, R. B., Kittaka, C., Neil, D., Chu, D. A., et al. (2005). Improving National Air Quality Forecasts with Satellite Aerosol Observations. *Bull. Amer. Meteorol. Soc.* 86, 1249–1262. doi:10.1175/bams-86-9-1249

Chen, R., Peng, R. D., Meng, X., Zhou, Z., Chen, B., and Kan, H. (2013). Seasonal Variation in the Acute Effect of Particulate Air Pollution on Mortality in the China Air Pollution and Health Effects Study (CAPES). *Sci. Total Environ.* 450-451, 259–265. doi:10.1016/j.scitotenv.2013.02.040

Chen, Z., Chen, D., Zhao, C., Kwan, M.-p., Cai, J., Zhuang, Y., et al. (2020). Influence of Meteorological Conditions on $PM_{2.5}$ Concentrations across China: A Review of Methodology and Mechanism. *Environ. Int.* 139, 105558. doi:10.1016/j.envint.2020.105558

Chen, Z. H., Cheng, S. Y., Li, J. B., Guo, X. R., Wang, W. H., and Chen, D. S. (2008). Relationship between Atmospheric Pollution Processes and Synoptic Pressure Patterns in Northern China. *Atmos. Environ.* 42, 6078–6087. doi:10.1016/j.atmosenv.2008.03.043

Delfino, R. J., Sioutas, C., and Malik, S. (2005). Potential Role of Ultrafine Particles in Associations between Airborne Particle Mass and Cardiovascular Health. *Environ. Health Perspect.* 113, 934–946. doi:10.1289/ehp.7938

Deng, X., Cao, W., Huo, Y., Yang, G., Yu, C., He, D., et al. (2019). Meteorological Conditions during a Severe, Prolonged Regional Heavy Air Pollution Episode in Eastern China from December 2016 to January 2017. *Theor. Appl. Climatol.* 135, 1105–1122. doi:10.1007/s00704-018-2426-4

Deng, X., Shi, C., Wu, B., Chen, Z., Nie, S., He, D., et al. (2012). Analysis of Aerosol Characteristics and Their Relationships with Meteorological Parameters over Anhui Province in China. *Atmos. Res.* 109-110, 52–63. doi:10.1016/j.atmosres.2012.02.011

Ding, Y., and Liu, Y. (2014). Analysis of Long-Term Variations of Fog and Haze in China in Recent 50 Years and Their Relations with Atmospheric Humidity. *Sci. China Earth Sci.* 57, 36–46. doi:10.1007/s11430-013-4792-1

Gao, B., Guo, H., Wang, X.-M., Zhao, X.-Y., Ling, Z.-H., Zhang, Z., et al. (2012). Polycyclic Aromatic Hydrocarbons in $PM_{2.5}$ in Guangzhou, Southern China: Spatiotemporal Patterns and Emission Sources. *J. Hazard. Mater.* 239-240, 78–87. doi:10.1016/j.jhazmat.2012.07.068

Gao, M., Liu, Z., Zheng, B., Ji, D., Sherman, P., Song, S., et al. (2020). China's Emission Control Strategies Have Suppressed Unfavorable Influences of Climate on Wintertime $PM_{2.5}$ Concentrations in Beijing since 2002. *Atmos. Chem. Phys.* 20, 1497–1505. doi:10.5194/acp-20-1497-2020

Gramsch, E., Cáceres, D., Oyola, P., Reyes, F., Vásquez, Y., Rubio, M. A., et al. (2014). Influence of Surface and Subsidence thermal Inversion on $PM_{2.5}$ and Black Carbon Concentration. *Atmos. Environ.* 98, 290–298. doi:10.1016/j.atmosenv.2014.08.066

Gu, Y., Zhang, W., Yang, Y., Wang, C., Streets, D. G., and Yim, S. H. L. (2020). Assessing Outdoor Air Quality and Public Health Impact Attributable to Residential Black Carbon Emissions in Rural China. *Resour. Conservation Recycling* 159, 104812. doi:10.1016/j.resconrec.2020.104812

Guo, J.-P., Zhang, X.-Y., Wu, Y.-R., Zhaxi, Y., Che, H.-Z., La, B., et al. (2011). Spatio-temporal Variation Trends of Satellite-Based Aerosol Optical Depth in China during 1980-2008. *Atmos. Environ.* 45, 6802–6811. doi:10.1016/j.atmosenv.2011.03.068

Guo, J., He, J., Liu, H., Miao, Y., Liu, H., and Zhai, P. (2016). Impact of Various Emission Control Schemes on Air Quality Using WRF-Chem during APEC China 2014. *Atmos. Environ.* 140, 311–319. doi:10.1016/j.atmosenv.2016.05.046

Guo, J., Li, Y., Cohen, J. B., Li, J., Chen, D., Xu, H., et al. (2019). Shift in the Temporal Trend of Boundary Layer Height in China Using Long-Term (1979-2016) Radiosonde Data. *Geophys. Res. Lett.* 46, 6080–6089. doi:10.1029/2019GL082666

Han, S., Liu, J., Hao, T., Zhang, Y., Li, P., Yang, J., et al. (2018). Boundary Layer Structure and Scavenging Effect during a Typical winter Haze-Fog Episode in a Core City of BTH Region, China. *Atmos. Environ.* 179, 187–200. doi:10.1016/j.atmosenv.2018.02.023

He, J., Gong, S., Yu, Y., Yu, L., Wu, L., Mao, H., et al. (2017). Air Pollution Characteristics and Their Relation to Meteorological Conditions during 2014-2015 in Major Chinese Cities. *Environ. Pollut.* 223, 484–496. doi:10.1016/j.envpol.2017.01.050

Holt, J., Selin, N. E., and Solomon, S. (2015). Changes in Inorganic Fine Particulate Matter Sensitivities to Precursors Due to Large-Scale US Emissions Reductions. *Environ. Sci. Technol.* 49, 4834–4841. doi:10.1021/acs.est.5b00008

Igawa, M., Tsutsumi, M., Mori, T., and Okochi, H. (1998). Fogwater Chemistry at a Mountainside Forest and the Estimation of the Air Pollutant Deposition via Fog Droplets Based on the Atmospheric Quality at the Mountain Base. *Environ. Sci. Technol.* 32, 1566–1572. doi:10.1021/es970213x

Jacob, D. J., Waldman, J. M., Munger, J. W., and Hoffmann, M. R. (1984). A Field Investigation of Physical and Chemical Mechanisms Affecting Pollutant Concentrations in Fog Droplets. *Tellus B: Chem. Phys. Meteorology* 36, 272–285. doi:10.3402/tellusb.v36i4.14909

Ji, D., Li, L., Wang, Y., Zhang, J., Cheng, M., Sun, Y., et al. (2014). The Heaviest Particulate Air-Pollution Episodes Occurred in Northern china in January, 2013: Insights Gained from Observation. *Atmos. Environ.* 92, 546–556. doi:10.1016/j.atmosenv.2014.04.048

Jin, Q., Fang, X., Wen, B., and Shan, A. (2017). Spatio-temporal Variations of $PM_{2.5}$ Emission in China from 2005 to 2014. *Chemosphere* 183, 429–436. doi:10.1016/j.chemosphere.2017.05.133

Kang, H. Q., BZhuGao, J., He, Y., Wang, H., and Su, J. (2018). Cold Fronts -- a Potential Air Quality Threat over the Yangtze River Delta, China. *Atmos. Chem. Phys.*, 1–17. doi:10.5194/acp-2018-588-AC2

Kang, H., Zhu, B., Gao, J., He, Y., Wang, H., Su, J., et al. (2019). Potential Impacts of Cold Frontal Passage on Air Quality over the Yangtze River Delta, China. *Atmos. Chem. Phys.* 19, 3673–3685. doi:10.5194/acp-19-3673-2019-supplement

Li, Z., Lau, W. K. M., Ramanathan, V., Wu, G., Ding, Y., Manoj, M. G., et al. (2016). Aerosol and Monsoon Climate Interactions over Asia. *Rev. Geophys.* 54, 866–929. doi:10.1002/2015RG000500

Liu, F., Zhang, Q., Tong, D., Zheng, B., Li, M., Huo, H., et al. (2015). High-Resolution Inventory of Technologies, Activities, and Emissions of Coal-Fired Power Plants in China from 1990 to 2010. *Atmos. Chem. Phys.* 15, 18787. doi:10.5194/acp-15-13299-2015

Markovic, M. Z., VandenBoer, T. C., Baker, K. R., Kelly, J. T., and Murphy, J. G. (2014). Measurements and Modeling of the Inorganic Chemical Composition of fine Particulate Matter and Associated Precursor Gases in California's San Joaquin Valley during CalNex 2010. *J. Geophys. Res. Atmos.* 119, 6853–6866. doi:10.1002/2013jd021408

Miao, Y., Guo, J., Liu, S., Liu, H., Li, Z., Zhang, W., et al. (2017). Classification of Summertime Synoptic Patterns in Beijing and Their Associations with

Boundary Layer Structure Affecting Aerosol Pollution. *Atmos. Chem. Phys.* 17, 3097–3110. doi:10.5194/acp-17-3097-2017

Ni, Z.-z., Luo, K., Zhang, J.-x., Feng, R., Zheng, H.-x., Zhu, H.-r., et al. (2018). Assessment of winter Air Pollution Episodes Using Long-Range Transport Modeling in Hangzhou, China, during World Internet Conference, 2015. *Environ. Pollut.* 236, 550–561. doi:10.1016/j.envpol.2018.01.069

Pasch, A. N., Macdonald, C. P., Gilliam, R. C., Knoderer, C. A., and Roberts, P. T. (2011). Meteorological Characteristics Associated with PM$_{2.5}$ Air Pollution in Cleveland, Ohio, during the 2009-2010 Cleveland Multiple Air Pollutants Study. *Atmos. Environ.* 45, 7026–7035. doi:10.1016/j.atmosenv.2011.09.065

Pei, L., Yan, Z., Sun, Z., Miao, S., and Yao, Y. (2018). Increasing Persistent Hazes in Beijing: Potential Impacts of Weakening East Asian Winter Monsoons Associated with Northwestern Pacific SST Trend since 1900. *Atmos. Chem. Phys.* 18, 3173–3183. doi:10.5194/acp-2017-757

Peters, A., Goldstein, I. F., Beyer, U., Franke, K., Heinrich, J., Dockery, D. W., et al. (1996). Acute Health Effects of Exposure to High Levels of Air Pollution in Eastern Europe. *Am. J. Epidemiol.* 144, 570–581. doi:10.1093/oxfordjournals.aje.a008967

Podzimek, J. (1998). Aerosol Particle Scavenging by Fog and Haze Droplets. *Stud. Geophys. Geod.* 42, 540–560. doi:10.1023/A:1023305423337

Pope, C. A., and Dockery, D. W. (2006). Health Effects of Fine Particulate Air Pollution: Lines that Connect. *J. Air Waste Manag. Assoc.* 56, 709–742. doi:10.1080/10473289.2006.10464485

Satheesh, S. K. (2002). Radiative Forcing by Aerosols over Bay of Bengal Region. *Geophys. Res. Lett.* 29, 40–41. doi:10.1029/2002GL015334

Shi, C. E., Nduka, I. C., Yang, Y., Huang, Y., Yao, R., Zhang, H., et al. (2019). Characteristics and Meteorological Mechanisms of Transboundary Air Pollution in a Persistent Heavy PM$_{2.5}$ Pollution Episode in Central-East China. *Atmos. Environ.* 223, 117239. doi:10.1016/j.atmosenv.2019.117239

Shi, C., Yuan, R., Wu, B., Meng, Y., Zhang, H., Zhang, H., et al. (2018). Meteorological Conditions Conducive to PM$_{2.5}$ Pollution in winter 2016/2017 in the Western Yangtze River Delta, China. *Sci. Total Environ.* 642, 1221–1232. doi:10.1016/j.scitotenv.2018.06.137

Su, T., Li, Z., Li, C., Li, J., Han, W., Shen, C., et al. (2020). The Significant Impact of Aerosol Vertical Structure on Lower Atmosphere Stability and its Critical Role in Aerosol-Planetary Boundary Layer (PBL) Interactions. *Atmos. Chem. Phys.* 20, 3713–3724. doi:10.5194/acp-20-3713-2020

Sun, Y., Wang, Z., Fu, P., Jiang, Q., Yang, T., Li, J., et al. (2013). The Impact of Relative Humidity on Aerosol Composition and Evolution Processes during Wintertime in Beijing, China. *Atmos. Environ.* 77, 927–934. doi:10.1016/j.atmosenv.2013.06.019

Waldman, J. M., and Hoffmann, M. R. (1987). *Depositional Aspects of Pollutant Behavior in Fog and Intercepted Clouds [M].* ISBN: 9780841209831.

Wang, H., Miao, Q., Shen, L., Yang, Q., Wu, Y., and Wei, H. (2021a). Air Pollutant Variations in Suzhou during the 2019 Novel Coronavirus (COVID-19) Lockdown of 2020: High Time-Resolution Measurements of Aerosol Chemical Compositions and Source Apportionment. *Environ. Pollut.* 271, 116298. doi:10.1016/j.envpol.2020.116298

Wang, H., Pei, Y., Yin, Y., Shen, L., Chen, K., Shi, Z., et al. (2021c). Observational Evidence of Lightning-Generated Ultrafine Aerosols. *Geophys. Res. Lett.* 48, e2021GL093771. doi:10.1029/2021gl093771

Wang, H., Tan, Y., Zhang, L., Shen, L., Zhao, T., Dai, Q., et al. (2021b). Characteristics of Air Quality in Different Climatic Zones of China during the COVID-19 Lockdown. *Atmos. Pollut. Res.* 12, 101247. doi:10.1016/j.apr.2021.101247

Wang, J., Zhang, M., Bai, X., Tan, H., Li, S., Liu, J., et al. (2017). Large-scale Transport of PM$_{2.5}$ in the Lower Troposphere during winter Cold Surges in China. *Sci. Rep.* 7, 13238. doi:10.1038/s41598-017-13217-2

Wang, L., Zhang, N., Liu, Z., Sun, Y., Ji, D., and Wang, Y. (2014). The Influence of Climate Factors, Meteorological Conditions, and Boundary-Layer Structure on Severe Haze Pollution in the Beijing-Tianjin-Hebei Region during January 2013. *Adv. Meteorology* 2014, 1–14. doi:10.1155/2014/685971

Wang, M., Cao, C., Li, G., and Singh, R. P. (2015). Analysis of a Severe Prolonged Regional Haze Episode in the Yangtze River delta, China. *Atmos. Environ.* 102, 112–121. doi:10.1016/j.atmosenv.2014.11.038

Wang, M. Y., Yim, S. H. L., Dong, G. H., Ho, K. F., and Wong, D. C. (2020). Mapping Ozone Source-Receptor Relationship and Apportioning the Health Impact in the Pearl River Delta Region Using Adjoint Sensitivity Analysis. *Atmos. Environ.* 222, 117026. doi:10.1016/j.atmosenv.2019.117026

Wang, X., Chen, J., Sun, J., Li, W., Yang, L., Wen, L., et al. (2014). Severe Haze Episodes and Seriously Polluted Fog Water in Ji'nan, China. *Sci. Total Environ.* 493 (15), 133–137. doi:10.1016/j.scitotenv.2014.05.135

Wang, Z., Liu, X., Xie, X., and Xie, X. M. (2016). Effects of Strong East Asian Cold Surges on Improving the Air Quality over Mainland China. *Atmosphere* 7, 38. doi:10.3390/atmos7030038

Wei, Y., Cao, X. N., Tang, X. L., Shen, L. J., Lin, T., He, D. W., et al. (2017). Urban fine Particulate Matter (PM$_{2.5}$) Exposure Destroys Blood-Testis Barrier (BTB) Integrity through Excessive ROS-Mediated Autophagy. *Toxicol. Mech. Methods* 28, 302–319. doi:10.1080/15376516.2017.1410743

Winker, D. M., Vaughan, M. A., Omar, A., Hu, Y., Powell, K. A., Liu, Z., et al. (2009). Overview of the CALIPSO Mission and CALIOP Data Processing Algorithms. *J. Atmos. Ocean. Tech.* 26, 2310–2323. doi:10.1175/2009JTECHA1281.1

Wu, X., Chen, B., Wen, T., Habib, A., and Shi, G. (2020). Concentrations and Chemical Compositions of PM$_{10}$ during Hazy and Non-hazy Days in Beijing. *J. Environ. Sci.* 87, 1–9. doi:10.1016/j.jes.2019.03.021

Xu, J., Chang, L., Yan, F., and He, J. (2017). Role of Climate Anomalies on Decadal Variation in the Occurrence of Wintertime Haze in the Yangtze River Delta, China. *Sci. Total Environ.* 599-600, 918–925. doi:10.1016/j.scitotenv.2017.05.015

Xu, J., Yan, F., Xie, Y., Wang, F., Wu, J., and Fu, Q. (2015). Impact of Meteorological Conditions on a Nine-Day Particulate Matter Pollution Event Observed in December 2013, Shanghai, China. *Particuology* 20, 69–79. doi:10.1016/j.partic.2014.09.001

Xu, Y., and Zhu, X. (2017). Recognizing Dew as an Indicator and an Improver of Near-Surface Air Quality. *Adv. Meteorology* 2017, 1–9. doi:10.1155/2017/3514743

Yang, J., Xie, Y.-J., Shi, C.-E., Liu, D.-Y., Niu, S.-J., and Li, Z.-H. (2012). Ion Composition of Fog Water and its Relation to Air Pollutants during Winter Fog Events in Nanjing, China. *Pure Appl. Geophys.* 169, 1037–1052. doi:10.1007/s00024-011-0342-y

Yang, Y., Zheng, X., Gao, Z., Wang, H., Wang, T., Li, Y., et al. (2018). Long-Term Trends of Persistent Synoptic Circulation Event`s in Planetary Boundary Layer and Their Relationships with Haze Pollution in Winter Half Year over Eastern China. *J. Geophys. Res. Atmos.* 123, 10991–11007. doi:10.1029/2018JD028982

Yang, Y., Zheng, Z., Yim, S. Y. L., Roth, M., Ren, G., Gao, Z., et al. (2020). PM$_{2.5}$ Pollution Modulates Wintertime Urban Heat Island Intensity in the Beijing-Tianjin-Hebei Megalopolis, China. *Geophys. Res. Lett.* 47, e2019GL084288. doi:10.1029/2019gl084288

Zhang, J. P., Zhu, T., Zhang, Q. H., Li, C. C., Shu, H. L., Ying, Y., et al. (2012). The Impact of Circulation Patterns on Regional Transport Pathways and Air Quality over Beijing and its Surroundings. *Atmos. Chem. Phys.* 12, 5031–5053. doi:10.5194/acp-12-5031-2012

Zhang, Q., Quan, J., Tie, X., Li, X., Liu, Q., Gao, Y., et al. (2015). Effects of Meteorology and Secondary Particle Formation on Visibility during Heavy Haze Events in Beijing, China. *Sci. Total Environ.* 502, 578–584. doi:10.1016/j.scitotenv.2014.09.079

Zheng, Z., Li, Y., Wang, H., Ding, H., Li, Y., Gao, Z., et al. (2019). Re-evaluating the Variation in Trend of Haze Days in the Urban Areas of Beijing during a Recent 36-year Period. *Atmos. Sci. Lett.* 20, e878. doi:10.1002/asl.878

Zheng, Z., Ren, G., Wang, H., Dou, J., Gao, Z., Duan, C., et al. (2018). Relationship between Fine-Particle Pollution and the Urban Heat Island in Beijing, China: Observational Evidence. *Boundary-layer Meteorol.* 169, 93–113. doi:10.1007/s10546-018-0362-6

Zhou, W., Tie, X., Zhou, G., and Liang, P. (2015). Possible Effects of Climate Change of Wind on Aerosol Variation during winter in Shanghai, China. *Particuology* 20, 80–88. doi:10.1016/j.partic.2014.08.008

Zhu, J., Liao, H., and Li, J. (2012). Increases in Aerosol Concentrations over Eastern China Due to the Decadal-Scale Weakening of the East Asian Summer Monsoon. *Geophys. Res. Lett.* 39, a–n. doi:10.1029/2012GL051428